Draft version February 1, 2008
Preprint typeset using LaTeX style emulateapj v. 14/09/00

arXiv:astro-ph/0111104v1 6 Nov 2001

CONFRONTATION OF INTRACLUSTER AND INTERSTELLAR GAS IN CLUSTER-CENTERED ELLIPTICAL GALAXIES: M87 IN VIRGO AND NGC 4874 IN COMA

Fabrizio Brighenti[1,2] & William G. Mathews[1]
[1]University of California Observatories/Lick Observatory, Board of Studies in Astronomy and Astrophysics,
University of California, Santa Cruz, CA 95064
mathews@lick.ucsc.edu
[2]Dipartimento di Astronomia, Università di Bologna, via Ranzani 1, Bologna 40127, Italy
brighenti@bo.astro.it

Draft version February 1, 2008

ABSTRACT

The evolution of hot interstellar gas in cluster-centered cD galaxies and the inflow of gas from the surrounding galaxy clusters are strongly coupled. Cooling flows arise inside the cD galaxy because the deep stellar potential and stellar mass loss increase the gas density and decrease the radiative cooling time within the galaxy. Recent X-ray observations of M87 in the Virgo cluster and NGC 4874 in Coma reveal that the gas temperature beyond about 50 kpc from these cD galaxies is comparable to the virial temperature of the cluster, 3 or 9 keV respectively, but within the optical galaxy the temperature drops to the galactic virial temperature ~ 1 keV. We show that these steep thermal gradients on galactic scales follow naturally from the usual cooling inflow assumptions without recourse to thermal conductivity. However, most of the gas must radiatively cool ("dropout") before it flows to the galactic core, i.e. the gas must be multiphase. The temperature and density profiles observed in M87 and NGC 4874 can be matched with approximate gas dynamical models calculated over several Gyrs with either globally uniform or centrally concentrated multiphase mass dropout. Recent *XMM* observations of M87 indicate single phase flow at every radius with no apparent radiative cooling to low temperatures. Gas dynamical models can be made consistent with single phase flow for $r \gtrsim 10$ kpc, but to avoid huge central masses of cooled gas, we assume that some distributed cooling dropout occurs near the center of the flow where the gas temperature is $T \sim 1$ keV. The evidence in X-ray spectra for multiphase cooling beginning at lower temperatures ~ 1 keV may be less apparent than for higher temperatures and may have escaped detection. However, even if the mass of cooled gas is distributed within $r \lesssim 10$ kpc, it is necessary that the mass of cooled gas not conflict with dynamical mass to light determinations. Because of small deviations from true steady state flow, we find that the standard decomposition methods used by X-ray observers to determine the mass flow $\dot{M}(r)$ may fail rather badly, particularly when the mass dropout decreases with radius in the flow. For this case the decomposition procedure gives the usual cooling flow result, $\dot{M} \propto r$, which is quite unlike the true variation of $\dot{M}(r)$ in our computed models.

Subject headings: galaxies: elliptical and lenticular – galaxies: active – galaxies: cooling flows – galaxies: radio – X-rays: galaxies – X-rays: galaxy clusters

1. INTRODUCTION

Both galaxy clusters and individual early-type galaxies contain virialized hot gas in which the radiative cooling time is much less than the Hubble time. According to the standard interpretation, as hot gas loses energy by emitting the X-radiation we observe, it slowly migrates inward. Since these "cooling flows" are nearly in hydrostatic equilibrium in the cluster or galactic potential, the temperature and density profiles measured in the hot gas can be used to determine the underlying mass distribution. For this reason it is particularly interesting to study cooling flows in galaxies since we already have information about the mass distribution from optical studies within the half-light radius r_e where the contribution of dark matter to the total mass is small.

Our objective in the calculations discussed here is to determine the nature of the interaction between cluster and interstellar gas in bright cD galaxies centrally located in galaxy clusters. In our previous studies of X-ray luminous massive elliptical galaxies located in small galaxy groups (e.g. Brighenti & Mathews 1999), we have assumed that the interstellar and circumgalactic gas have been relatively unperturbed since the galaxy first formed. By following the growth of cosmological perturbations, including star formation and feedback, we can compute the gas flow over most of the Hubble time, successfully reproducing the radial dependence of hot gas density, temperature and abundance currently observed in massive group-centered elliptical galaxies. However, the hot gas surrounding cluster-centered elliptical galaxies has a much higher cluster virial temperature. As cluster gas flows into the central cD or elliptical galaxy, the interstellar gas is perturbed from that of more isolated or group-centered ellipticals, providing a useful test of the many parameters involved in these calculations. In particular, cluster-centered cD galaxies provide an excellent venue to explore the nature or reality of the mass "dropout" hypothesis, i.e. that the hot gas is multiphase, having locally varying densities and cooling times, so that it cools ("drops out") throughout a large volume of the cooling flow. Unfortunately, the long term evolution of ambient cluster gas around cluster-centered cD galaxies is uncertain because of the likelihood of disruptive mergers in the cluster environment. Nevertheless, much can be learned if we assume that the cluster gas as currently observed near the cD galaxy has been relatively stable for times longer than several sound-crossing times, typically several Gyrs.

In the traditional interpretation of cooling flows, it is assumed that the X-ray luminosity L_x reflects energy lost from the hot gas which is not balanced by a heating source. As the radiating gas loses energy and slowly migrates toward the potential minimum, it is maintained near the local virial temperature by Pdv compression. In the simplest (single phase) cooling flows all the gas cools rapidly at very center of the E or cD galaxy where the gas density and radiative emission are greatest. This model clearly fails since strong localized central peaks of thermal X-ray emission are not generally observed and the total mass of cooled gas concentrated in the central regions would increase the stellar velocity dispersions considerably above those observed (e.g. Thomas 1986; White & Sarazin 1987; Mathews & Brighenti 2000). To alleviate these difficulties, it has been fashionable for many years to assume that the hot gas is "multiphase" and therefore cools throughout a larger volume, depositing its mass in a less concentrated manner (Nulsen 1986; Thomas et al. 1987; Allen et al. 2001).

Multiphase cooling can be incorporated into the equation of continuity for cooling flows with a mass sink term:

$$\frac{\partial \rho}{\partial t} + \frac{1}{r^2}\frac{\partial}{\partial r}(r^2 \rho u) = \alpha_* \rho_* - q\frac{\rho}{t_{cool}}. \tag{1}$$

The source term proportional to the stellar density ρ_* represents stellar mass ejected from evolving stars. The following dropout or sink term simply removes gas from the flow at a rate characterized by the local radiative cooling time at constant pressure $t_{cool} = 5 m_p kT/2\mu\rho\Lambda$. This term is preceded by a dimensionless coefficient $q(r) \lesssim 1$ which is adjusted to best fit the observed X-ray surface brightness and other observations. We recognize the *ad hoc* character of this sink term, particularly in view of the well known failure of linear analysis to find instability in cooling flows (e.g. Balbus & Soker 1989). Nevertheless, the compelling astrophysical arguments against concentrated cooling at the center of the flow suggest either some form of distributed mass dropout as in Equation (1) or an equally *ad hoc* heating effect that supplies thermal energy without driving a strong global wind. Ironically, we have recently shown (Brighenti & Mathews 2002) that nonlinear density perturbations and subsequent thermal instabilities occur naturally in cooling flows that are decelerated by heating or additional non-thermal pressure near the center of the flow.

To estimate q we use the recent compilation of six well-observed cluster cooling flows from Allen et al. (2001) for which the local radiative cooling times are linear functions of radius, $t_{cool} = t_{cool,b}(r/r_b)$, for $r < r_b$. Since $r_b \sim 40 - 120$ kpc is much greater than the central galactic half-light radius $r_e \sim 10$ kpc, $\alpha_* \rho_* \ll \rho/t_{cool}$ beyond the central galaxy. Multiplying the equation above by $4\pi r^2 dr$, assuming quasi-steady state flow and substituting $\rho = 5 m_p kT/2\mu t_{cool}\Lambda$,

$$d\dot{M} = d(\rho u 4\pi r^2) = -q\frac{20\pi m_p kT}{2\mu\Lambda}\frac{r^2 dr}{t_{cool}^2}. \tag{2}$$

We see that $t_{cool} \propto r$ implies $\dot{M} \propto r$ as verified by Figure 6 of Allen et al. who determine consistent mass flow or dropout profiles $\dot{M}(r)$ from both spectroscopic and surface brightness observations. Integrating this equation to $r = r_b$ and rearranging we find

$$q = \frac{2\mu\Lambda(T)}{20\pi m_p kT}\frac{\dot{M}(r_b) t_{cool,b}^2}{r_b^3} \tag{3}$$

which is constant in $r < r_b$ in this simple approximation. Using data from the six well-observed clusters in Allen et al., we find $\langle q \rangle \approx 0.3 - 0.6$. But the implication that $t_{cool} \propto r$ requires $\dot{M} \propto r$ is very sensitive to the steady state assumption as we show in Section 4 below.

Recently, *XMM* and *Chandra* have revealed new and unexpected attributes of galactic and cluster cooling flows (McNamara et al. 2000; Fabian et al. 2001; Fabian 2001). In several cluster cooling flows there is spectroscopic evidence for only partial cooling, down to ~ 2 keV, but no further (e. g. Peterson et al. 2001; Tamura et al. 2001; Kaastra et al. 2001; Molendi & Pizzolato 2001; Xu et al.

2001). This has led some to question the reality of the q-term in the equation of continuity and to postulate instead some as yet poorly understood form of heating (e.g. Tucker & Rosner 1983; Binney & Tabor 1995; Tucker & David 1997; Ciotti & Ostriker 2000; Soker et al. 2001). Although the traditional mass dropout hypothesis is being challenged, at the present time there is no accepted alternative model with heating that can be compared in detail with observations.

Nevertheless, some recent observations continue to support the reality of traditional cooling flows. Buote (2000, 2001) finds evidence of widespread X-ray absorption from warm gas at $T \sim 10^6$ K in many cooling flows including M87. FUSE observations of cluster A2597 have detected the OVI doublet from gas at $T \sim 3 \times 10^5$ K corresponding to a lower than expected $\dot{M}$, but OVI lines are undetected in A1795 (Oegerle et al. 2001). Similar FUSE observations of elliptical galaxies find OVI emission consistent with (but possibly somewhat less than) the expected mass cooling rate $\dot{M}$ and the usual multiphase cooling flow model (e.g. Bregman et al. 2001). Perhaps some OVI line emission may have escaped detection because of broadening by turbulent velocities. Finally, Canizares et al. (1982) discovered line emission in M87 corresponding to temperatures of a few 10^6 K which they interpret at radiatively cooling gas. Although the evidence is somewhat contradictory at present, we adopt provisionally the traditional assumption that cooling flows do in fact cool and seek values of $q(r)$ for cluster-centered cD galaxies that agree best with recent X-ray observations.

In the following we describe the transition flow as cluster gas enters M87 from the Virgo cluster and NGC 4874 from the Coma cluster, both of which have been observed by *XMM* and/or *Chandra*. Remarkably, there is little evidence that the powerful, ongoing AGN in M87, with its jet and radio lobes, are heating the cooling flow at small galactic radii (e.g. Fabian 2001; Soker et al. 2001). Indeed, we demonstrate below that the gas temperature, density and entropy profiles in M87/Virgo and NGC 4874/Coma are approximately consistent with a normal galactic-scale cooling flows, requiring little or no additional local heating. The interaction of cluster and galactic gas has been discussed previously by Thomas (1986), Meiksin (1990) and Bertin & Toniazzo (1995).

2. M87 IN VIRGO

2.1. *M87/Virgo Mass Distribution*

Using ROSAT data, Nulsen & Böhringer (1995) determined the azimuthally averaged mass distribution of the Virgo cluster within 50′ (247 kpc at distance $d = 17$ Mpc) of M87. Their best-fitting model has a total density structure

$$\rho \propto [1 + (r/a)^2]^{-1} \tag{4}$$

and mass profile

$$M_{virgo}(r) = M_o[r/a + \arctan(r/a)] \tag{5}$$

where $a = 47.6$ kpc and $M_o = 5.90 \times 10^{12}\ M_\odot$. The mass distribution is sensitive to the observed gas temperature variation $T(r)$ which for $r \gtrsim 85$ kpc is approximately isothermal at ~ 2.8 keV (3.2×10^7 K) (Nulsen & Böhringer 1995). The observed X-ray surface brightness in Virgo is more consistent with this $M_{virgo}(r)$ than with an NFW mass profile, although the difference is not great.

We determine the stellar mass distribution in M87 (NGC 4486) from the B-band surface brightness μ_B derived from the μ_V and B-V photometry of Goudfrooij et al. (1994) within $r = 132''$. Beyond this radius we use the V-band photometry of Schombert (1986) corrected to μ_B with B-V = 0.80, and brightened by $\delta V = 0.5$ to agree with the Goudfrooij et al. data in $r \lesssim 132''$. The B-band surface brightness μ_B is transformed to surface mass density using $M/L_B = 8.2$ (van der Marel 1991). (Note that Faber et al. (1997) find a much larger value, $M/L_B = 23$.) The stellar mass density, found by solving Abel's equation, can be fit with

$$\rho_*(r) = (r/r_b)^{-1}[1+(r/r_c)^{1.7}]^{-1}[1+(r/r_d)]^{-0.4} \quad M_\odot\ \mathrm{pc}^{-3} \tag{6}$$

where $r_b = 4.379$, $r_c = 1.513$ and $r_d = 15$ kpc. The stellar mass distribution $M_{*,87}$ differs from a de Vaucouleurs profile because of the unusually large core (break) radius in M87 and an outer cD envelope of moderate brightness. The potential is dominated by stars within 40 kpc. The density profile in Equation (6) is in good agreement with that of van der Marel (1994). Finally, we assume that M87 is surrounded by a dark galactic halo with an NFW profile and total mass $M_{87,nfw} = 1.0 \times 10^{13}\ M_\odot$. While it is unclear if it is necessary to append a separate dark halo to the central cD, we note that dynamical models of cluster-centered E galaxies have been unable to reproduce their massive cD envelopes (e.g. Dubinski 1998). Fortunately, the mass $M_{87,nfw}$ has only a minor influence on our results because of the enormous mass of the Virgo cluster at every radius beyond the stellar half-light radius.

2.2. *Computational Procedure*

Each gas dynamical calculation begins with a determination of the gas density profile of isothermal intracluster gas in hydrostatic equilibrium in the Virgo potential defined by $M_{virgo}(r)$. At cosmic time t_i the central galaxy and its dark halo are inserted into the Virgo environment. After this time stellar mass loss contributes to the local gas at a rate $\alpha_*(t)\rho_*(r)$ gm s^{-1} cm^{-3}. Here $\alpha_*(t) = \alpha_{*,n}(t/t_n)^{-1.3}$ s^{-1}, appropriate for a nearly coeval burst of star formation at high redshift where $\alpha_{*,n} = 4.7 \times 10^{-20}$ s^{-1}, and $t_n = 13$ Gyrs is the present age of the universe. Gas within the optical galaxy is heated by Type Ia supernovae which occur at a rate $\mathrm{SNu}(t) = \mathrm{SNu}(t_n)(t_n/t)$ where $\mathrm{SNu}(t_n) = 0.06$ supernovae per $10^{10}\ L_B$ per 100 years. These stellar mass loss and supernova rates are consistent with X-ray observations of massive E galaxies such as NGC 4472 that are not centered in large clusters (e.g. Brighenti & Mathews 1999).

After time t_i, as the hot intracluster gas flows into the optical galaxy, it is cooled by radiation losses and mass ejected from evolving stars. Since mass-losing stars orbit rapidly through the hot gas, we expect instabilities to thermally mix stellar and ambient gases. This assumption is confirmed by negative abundance gradients of α-elements observed in M87 (Molendi & Gastaldello 2001) which cannot have been produced by Type Ia supernovae. In large galaxies such as M87, the global potential is so deep that Type Ia heating has rather little effect on the thermal budget of the gas; the SNIa luminosity at t_n,

$L_{SNIa} = 1.6 \times 10^{41}$ erg s^{-1}, is considerably less than the total X-ray emission L_x from within the optical image of M87. Following a brief transient (< 1 Gyr) just after M87 is introduced into the Virgo environment, the gas flow settles into a subsonic, but secularly changing flow. The gas dynamical equations that we use are identical to those discussed in Brighenti & Mathews (1999) to which we refer the reader for further details. The equations are solved with a considerably modified 1D spherical version of the ZEUS code (Stone & Norman 1992) using 360 logarithmically increasing zones beginning with a central zone of size 15 pc and extending to 2.1 Mpc. The appropriate initial temperature $T(t_i)$ for Virgo gas at time t_i depends somewhat on the nature of the assumed mass dropout profile $q(r)$. If distributed mass dropout is small at large radii, i.e. $q \approx 0$, the isothermal temperature $T(t_i)$ should be close to that observed by Nulsen & Böhringer. But if $q \approx 1$ at large radii, the temperature of the background flow $T(t_i)$ must exceed that observed, which is a weighted average over both background and cooling regions.

The factors that influence the radial variation of gas density and temperature within the optical galaxy at time $t_n = 13$ Gyrs are: (1) the assumed mass dropout profile $q(r)$ and therefore $T(t_i)$, (2) the central gas density $n(r = 0, t_i)$ of the hydrostatic cluster gas distribution just before the galaxy is inserted, (3) the time elapsed since this initial configuration $t_n - t_i$, (4) the specific stellar mass-loss rate α_* and (5) thermal conductivity. As we show below, our computed values of $n(r, t_n)$ and $T(r, t_n)$ inside and near M87 are only weakly sensitive to the time $t_n - t_i$ over which the gas flow evolves after the initial setup, provided $t_n - t_i$ is larger than ~ 3 Gyr, i.e. several sound crossing times. The time $t_n - t_i$ can be regarded as the (unknown) interval since the last major merger event in Virgo when the gas density and temperature may have changed appreciably. While it is unlikely that α_* varies strongly with galactic radius, the normalization coefficient $\alpha_{*,n}$ can influence $n(r, t_n)$ and $T(r, t_n)$ somewhat. It is unlikely that thermal conduction plays an important role in the thermal structure of M87/Virgo (e.g. Saito & Shigeyama 1999). We find that thermal conduction at $\gtrsim 0.1$ of the Spitzer (or saturated) rate cannot occur since the gas temperature would be nearly isothermal at $T \approx T(t_i) \sim 3$ keV even within ~ 30 kpc and this is not observed. Thermal conduction can help reduce the total mass of cooled gas in the central regions of M87, but this requires that the conductivity be reduced by a carefully chosen factor that preserves the observed temperature profile (e.g. Bertschinger & Meiksin 1986). Therefore, in our discussion below we concentrate mostly on the remaining factor that influences the currently observed gas density and temperature distributions: the mass dropout coefficient $q(r)$.

2.3. *Results*

In Figures 1 and 2 we compare the observed gas density and temperature profiles in M87/Virgo with results of our gas dynamical calculations. Unless otherwise noted, all calculations begin at cosmic time $t_i = 6$ Gyrs and continue to the present time $t_n = 13$ Gyrs. At time t_i the hot cluster gas is in hydrostatic equilibrium in the mass distribution $M_{virgo}(r)$. The cluster gas is isothermal at $T(t_i) = 3$ keV (3.5×10^7 K) for models with $q(r) \ll 1$ at $r \gtrsim 20$ kpc and $T(t_i) = 3.4$ keV (4.0×10^7 K) for (globally multiphase) models with $q = 1$. The central gas density $n(0, t_i) = 0.003$ cm^{-3} is chosen to agree with X-ray surface brightness observations at radii far beyond the optical extent of M87.

If $q = 1$ throughout the flow, about half of the total X-radiation comes from the cooling elements and the rest comes from the background flow. We distinguish these two sources of emission in Figures 1 and 2 by plotting both the background density $n_h(r)$ (light solid line) and the density $n(r)$ that would be determined from the combined emission from background and cooling regions (heavy solid line). This latter $n(r)$ can be compared with the density profile determined from observations. In the temperature plots we show three temperatures: the temperature $T_h(r)$ of the hot background gas flow at radius r (dotted lines), the mean local emission-weighted temperature $T(r)$ including both background and cooling gas (light solid lines), and the emission-weighted temperature $T(R)$ which is $T(r)$ averaged along the line of sight, including emission from both background flow and cooling gas (heavy solid lines). R is the projected radius. If $dT/dr > 0$, $T(R)$ is greater than $T(r)$ for $r = R$ because emission from hotter gas along the line of sight is included in the weighted average $T(R)$. The temperature $T(R)$ reported by observers is not simply an emission-weighted mean along the line of sight, but is derived by fitting single temperature (1T) or composite temperature (2T or 1T + CF) XSPEC models to the projected X-ray spectrum. Nevertheless, in the following discussion we assume that our computed $T(R)$ – which includes effects of $dT/dr \neq 0$ as well as cooling dropout when $q \neq 0$ – can be directly compared with observed temperatures.

Over time $t_n - t_i = 13 - 6 = 7$ Gyrs, cooling flows do not form in Virgo without M87. If the evolution of the cluster gas after t_i is calculated without M87, we find that $T(R)$ at time t_n rises from ~ 1.5 keV at the center, reaches 2.6 keV at $r = 100$ kpc, then slowly rises toward $T(t_i)$. The gas density is similar to $n(r, t_i)$ for $r \gtrsim 50$ kpc, but within this radius it is much less than observed, $n(r, t_n) \lesssim 0.01$ cm^{-3} and by time t_n no gas has cooled. However, when M87 is introduced at t_i, the central gas density and X-ray surface brightness increase both because of the locally deepened (stellar) potential and because of the addition of stellar mass loss. We find that the deep potential of M87 is sufficient to create a cooling flow in M87/Virgo even if stellar mass loss is absent; this is possible since the Virgo virial temperature is only 2 - 3 times larger than that of M87. Stellar mass loss further cools the cluster gas and increases its density as it flows into the optical galaxy, lowering the radiative cooling time.

2.3.1. *Gas Flow with Constant and Variable q*

Figure 1 shows the resulting density and temperature profiles for the $q = 1$ model in which cooling dropout occurs uniformly throughout the flow. The computed density variation $n(r)$ (heavy solid line) agrees quite well with the gas density observed in M87/Virgo. The density continues to rise in $r < 1$ kpc, where the observational data are sparse, but in this region it is likely that the magnetic field is high enough $\sim 100\mu$G to flatten the gas density profile. Owen, Eilek & Keel (1990) estimate a field of

$\sim 40\mu$G at $r = 2$ kpc. The projected model temperature profile $T(R)$ also agrees reasonably well with observed values but is somewhat lower for $r \lesssim 2$ kpc and $r \gtrsim 45$ kpc. M87 observations are more difficult near the center because of non-thermal X-radiation from the active nucleus (e.g. Böhringer et al. 2001; Molendi & Gastaldello 2001), which may explain some of the temperature discrepancy at small r, along with a variety of other possible explanations (see below). The failure of the $q = 1$ model to match observed temperatures beyond ~ 45 kpc suggests that q may be less than 1 in this region since the observed temperatures in Figure 1 increase toward that of the uncooled background gas $T_h(r)$ (dotted line) which is ~ 0.8 keV hotter than $T(R)$.

To explore variable mass dropout, we show in Figure 2 the results of a calculation with a cooling dropout that decreases with gas density and therefore galactic radius, $q = \exp[-0.05/n(r)]$, but which is otherwise identical to the solution shown in Figure 1. As a function of radius, $q \approx 1$, 0.5 and 0.1 at $r = 0.0$, 2.8 and 7.6 kpc respectively. The agreement with observed density is very good and $T(R)$ agrees adequately with observed values. It is interesting that the observed density $n(r)$ and temperature $T(R)$ profiles can be fit for either constant or spatially variable q, particularly for $r \gtrsim 10$ kpc. But the observed spectra of the two flows are quite different, as we discuss below.

Inside ~ 2 kpc in Figure 1 or ~ 10 kpc in Figure 2 the computed temperature $T(R)$ is somewhat lower than observed. It is unlikely that this discrepancy is due to shock heating by the M87 AGN or radio source. In our experience the principal long term consequence of local heating is to lower the central gas density with only a very small change in temperature. In any case, *Chandra* observations provide little or no direct evidence of shock heating in radio galaxies (e.g. Fabian 2000). Several possible explanations for this temperature discrepancy are explored in the additional $q = \exp[-0.05/n(r)]$ solutions shown in Figure 3. If the time since the initial M87/Virgo configuration $t_n - t_i$ is $\lesssim 4$ Gyrs, we find that both $T(R)$ and dT/dR are larger in $R \lesssim 10$ kpc. This is illustrated in Figure 3 with a solution at $t_n - t_i = 13 - 10 = 3$ Gyrs (long dashed lines) which is a poor fit to observed $n(r)$ and $T(r)$. However, for $t_n - t_i \gtrsim 4$ Gyrs all $T(R)$ profiles resemble that in Figure 2. Reducing the normalization of the stellar mass loss rate $\alpha_{*,n}$ by a factor of 2 also has a beneficial, but limited affect on $T(R)$ (short dashed line in Fig. 3). However, if the stellar mass to light ratio is twice that of van der Marel, $M/L_B = 16.4$ – and therefore in better agreement with the M/L_B of Faber et al. (1997) – the temperature profile is considerably improved (solid line). (Note: $\alpha_* \propto (M/L_B)^{-1}$ has been reduced by 2 in this model.)

In Figure 2 $T(R)$ is in excellent agreement with observations in $R \gtrsim 10$ kpc. In this region the gas is essentially single phase, $T_h(r) = T(r)$, and the full line of sight variation $\sim 2[T(R) - T(r)] \approx 0.4 - 0.7$ keV is comparable to the cooling flow temperature range $T_{max} - T_{min}$ in the XSPEC (Model C) analysis of Molendi & Pizzolato (2001) at $r \gtrsim 10$ kpc. The multiphase appearance is due entirely to contributions of various single phase temperatures along the line of sight. At smaller radii, $r \lesssim 10$ kpc, q increases, and $T(R)$ is reduced by contributions from gas that is cooling below 1 keV.

We have also repeated M87/Virgo calculations with no dropout at all, $q = 0$, so that all the gas cools right at the origin. The results of these calculations agree surprisingly well with observations at $r \gtrsim 1$ kpc, particularly if α_* is also lower. But there is a major problem. In $r \lesssim 1$ kpc both the gas density and temperature increase in the (point source) potential of the centrally cooled mass, producing a dense, luminous X-ray core. However, central masses $\gtrsim 10^{10}$ $M_\odot$ and central peaks in T and L_x are not typically observed, so cooling inflows without spatially distributed dropout are unrealistic.

2.3.2. *Multiphase flow in M87/Virgo*

The detailed shape of the density and temperature profiles in M87/Virgo can be adequately reproduced with either constant or variable q, but this degeneracy can be broken by examining the X-ray spectra of these models in more detail. If $q = 1$ as in Figure 1, the line and continuum X-ray spectrum in $r \gtrsim 20$ kpc should consist of two components of approximately equal flux: (1) a blend of emission from line of sight plasma at temperatures $T_h \sim 2.8 - 3.4$ keV, and (2) emission from regions cooling at every radius through all temperatures $T < T_h$. However, if $q \approx 0$ as in our variable q model beyond 10 kpc, $T(R)$ is determined by only the first of these two components. In the upper panel of Figure 4 we show approximate local spectra at $r = 30$ kpc for both constant and variable q models. For the $q = \exp[-0.05/n(r)]$ flow we use a single temperature (1T), solar abundance mekal model (using XSPEC version 11.0.1) at $T = 2.5$ keV. For the $q = 1$ model spectrum we combine two bolometrically equal components: a 3 keV 1T spectrum and a mekal cooling flow (CF) spectrum with $T_{max} = 3$ keV. The difference between the $q = 1$ and variable q spectra is most apparent near the Fe-L line complex near 1 keV which is broadened toward lower energies in the (1T + CF) spectrum for $q = 1$ flow.

The current observational evidence for truly multiphase gas in M87/Virgo is contradictory. Buote (2001) reanalyzed *ROSAT* PSPC data from M87/Virgo, including the important spectral range down to 0.2 keV, and concluded that a single temperature gas cannot explain the X-ray spectrum. Instead, Buote finds evidence of emission in the 0.2 - 0.4 keV band from warm ($T \sim 10^6$ K) gas in M87/Virgo at almost every radius $\lesssim 70$ kpc except, curiously, in the $r = 5 - 10$ kpc region where the multiphase flow appears to be suppressed. Buote also finds (oxygen edge) absorption in the 0.5 - 0.8 keV range throughout M87/Virgo consistent with absorption by the same warm gas that emits at lower energies. The mass of warm gas necessary for this absorption in M87 is enormous, comparable to the total mass of hot gas observed, and it is unclear why the warm gas would not cool further (see also Bonamente et al. 2001). An important part of Buote's argument, shown in his Figure 4, is that if data below 0.5 - 0.7 keV is neglected, as many authors have done, the absorbing foreground column N_H greatly exceeds the Galactic value; conversely, if the entire spectrum down to 0.2 keV is considered, the foreground N_H is approximately Galactic at every projected radius in M87/Virgo, but some warm gas absorption is required. Buote's *ROSAT* data cannot easily discriminate between spectra of two temperature plasma and and a single temperature with cooling elements.

This evidence for multiphase gas in M87/Virgo is not supported by *XMM* data analyzed by Böhringer et al. (2001) which are spectroscopically superior to *ROSAT*. When they attempted a multiphase solution by combining spectra from T_h with that of a cooling gas, Böhringer et al. found mass deposition rates of $\dot{M} \sim 10 \pm 5\ M_\odot$ yr^{-1} within 50 kpc and absorbing columns $N_H \sim 5 \times 10^{21}$ cm^{-2} that are about 30 times the Galactic value.

Molendi & Pizzolato (2001) have reanalyzed 0.5 - 4.0 keV *XMM* EPIC data from M87/Virgo and lend support to the conclusions of Böhringer et al.: (1) the only multiphase attributes apparent in M87/Virgo spectra are those introduced by the variation of single phase temperatures along the line of sight, and (2) there is no evidence for intrinsic multiphase gas that is cooling locally. In their best multiphase cooling flow (Model B), Molendi & Pizzolato find (1) that the (spectroscopic) total mass deposition rate in M87/Virgo is less than 0.5 $M_\odot$ yr^{-1}, at least an order of magnitude less than that expected from L_x, and (2) very large absorbing columns N_H. They suggest that earlier claims of large soft X-ray absorption are an artifact resulting from the multiphase assumption. But there remain problems with the model favored by Molendi & Pizzolato, Model C, in which the temperature range viewed along the sight is sufficient to account for the full temperature range observed at all R. They model this temperature range with a partial isobaric cooling flow from T_{max} to T_{min} rather than by integrating over the known $T(r)$ along the line of sight. But gas cannot just cool to some minimum temperature – ether locally as cooling dropout or during its radial flow – and accumulate there since that would eventually distort the entire spectrum toward this low temperature. This is the conundrum discussed by Fabian et al. (2001) who claim that "cooling flow" gas appears to cool to some intermediate temperature T_{min}, then disappear.

However, we must not overlook the *Einstein* FPCS observation of Fe XVII - Fe XXIV lines in the central $\sim 2'(\sim 10$ kpc) of M87 by Canizares et al. (1982) that reveal gas temperatures ranging from 3×10^7 K down to $2 - 4 \times 10^6$ K. The volume emission measure from cooling gas suggests a cooling rate of 3 - 4 $M_\odot$ yr^{-1}. This is clear evidence in support of the multiphase model, at least in this central region.

2.3.3. *Spectroscopic Evidence for Variable q*

Returning to Figure 4, the easily visible low-energy extension of the Fe-L line feature, which indicates cooling to very low temperatures, was evidently not seen at $r \sim 30$ kpc by Molendi & Pizzolato (2001) in their XMM spectra of M87. This is in agreement with our variable $q(r)$ model in which $q \approx 0$ in $r \gtrsim 10$ kpc. However, in their (preferred) Model C analysis of *XMM* data in which the temperature cools through a finite range, simulating the variation of T along the line of sight, Molendi & Pizzolato find temperature ranges of $1.0 < T < 1.8$ keV at $r = 3.9$ kpc and $1.4 < T < 1.9$ at $r = 7.5$ kpc. These narrow ranges are inconsistent with intrinsic multiphase cooling in this region, with the observations of Canizares et al. 1982, and with our variable q model. However, it may be more difficult to detect multiphase cooling when the gas cools from low temperatures, $T \sim 1$ keV, as in our variable q model within 10 kpc.

To illustrate this, in the lower panel of Figure 4 we use XSPEC (ver. 11.0.1) to compare intrinsic 0.2 - 3 keV spectra at $\sim$ 1 kpc, assuming solar abundances. The solid line shows the combined spectrum of a single temperature (1T) gas at $T_h = 0.95$ keV plus a cooling flow (CF) spectrum for $T = 0.95 \rightarrow 0.1$ keV, with equal normalizations. For comparison we show with a dotted line in Figure 4 the mekal spectrum of a single phase gas at the mean temperature of the 1T + CF flow, $T \approx 0.8$ keV (cf. Fig. 2). The difference between these two spectra is much less than that between 1T and (1T$_h$ + CF) spectra at $\sim$ 3 keV (upper panel) corresponding to $R = 30$ kpc where the Fe-L feature is widened by the cooling gas. To demonstrate conclusively that gas at $\sim$ 1 keV is not cooling to very low temperatures, it would be necessary to be confident of the relative strengths of the Fe-L lines in 0.7 - 1.0 keV which may not be possible at present. Alternatively, the line ratio OVII(0.574 keV)/OVIII(0.652 keV) increases with decreasing temperature below 1 keV (Landini & Monsignori Fossi 1990), which is apparent in Figure 4. However, OVII(0.574 keV)/OVIII(0.652 keV) could be artificially increased by oxygen-edge absorption (Boute 2001), which is a further possible complication. On balance, therefore, these spectroscopic considerations favor the variable $q(r)$ model for M87/Virgo, in which q becomes effectively nonzero only within 10 kpc where a multiphase spectrum would be expected, but which may be difficult to observe.

2.3.4. *Where is the Cooled Gas?*

A potentially serious problem with the variable q model is that the centrally concentrated mass dropout may conflict with the stellar mass to light ratio of M87. In his global dynamic models for M87, van der Marel (1991) found $M/L_B = 8.2$ while Faber et al. (1997) find $M/L_B = 23$ using the King method applied to the galactic core (Richstone & Tremaine 1986; Tremaine et al. 1994). In these estimates M/L_B is always assumed to be uniform with radius – which would not be expected if mass dropout is important. The discrepancy in M/L_B could indicate that dark dropout mass exists mostly within the M87 core, although van der Marel (1994) also finds a stellar $M/L_B = 8.2$ in stars near the central black hole and Merritt & Oh (1997) find $M/L_B = 11$. The black hole mass considered by van der Marel, $M_{bh} = 3 \times 10^9$, is only three times less than the total stellar mass $M_b = 1.0 \times 10^{10}$ $M_\odot$ within the core (or break) radius $r_b = 626$ pc (7.61$''$). This black hole mass is confirmed by observations of a thin HII disk in Keplerian rotation to within 4 pc of the center (Marconi et al. 1997; Macchetto et al. 1997).

Most of the dark matter deposited in the M87 core by the variable q solution occurs at very early times. To study this in more detail we use an "alternative" M87/Virgo model in which the initial evolution of M87 occurs outside Virgo and the galactic scale cooling flow deposits mass according to $q = \exp(-0.05/n)$. By time $t_i = 6$ Gyrs when M87 is inserted in Virgo, the total mass of cooled (dropped out) gas is already $M_{do} = 2.3 \times 10^{10}$ $M_\odot$ or $2.3 M_b$. At these early times our schematic model for galaxy evolution is very uncertain. Since the stars in M87 have significant metal enrichment, some of the enriched galactic hot gas that cooled at early times must have formed into second generations of old luminous stars observed today (Nulsen & Fabian 1997). But it is unclear how long cooled gas formed into optically luminous stars. Many authors have suggested that at the present time only low mass, optically dark stars are forming in cooling flows, but other lines of evidence, such as the stellar Hβ index, suggest that luminous stars continue to form at the present time (Mathews & Brighenti 1999). Furthermore, the precise value of the total mass of cooled gas at time t_i depends critically on the unknown cooling and merger history of M87 before t_i and whether or not $q = \exp(-0.05/n)$ applies at these early times, as we have assumed. By time $t_n = 13$ Gyrs, in the variable q flow 5.3×10^{10} $M_\odot$ has cooled.

If the cooling dropout hypothesis is correct, the currently observed stellar mass to light ratio must reflect in part a contribution from cooled gas. If luminous stars form continuously from cooled gas, the mass to light ratio could in principle be similar to that of the old stellar population, although an exact match seems unlikely. On the other hand, if only non-luminous stars formed in our $q = \exp(-0.05/n)$ flow, then at time $t_i = 6$ Gyrs M/L_B would have already increased to 18 within the break radius r_b, ignoring passive cosmological luminosity evolution. By time $t_n = 13$ Gyrs, M/L_B within r_b increases further to 28 which is unacceptably high. Notice, however, that in our models the mass dropout continues to increase with rising gas density in $r \lesssim r_b$ where about half of the dropout occurs for the variable q flow. It is more likely that the gas density in M87 levels off in $r \lesssim 1$ kpc similar to other large elliptical galaxies in Virgo (e.g. Brighenti & Mathews 1997), possibly due to large central magnetic fields or the central AGN. If so, mass dropout within r_b would be much reduced. More generally, the success of the variable q flow does not depend critically on the exact profile of $q(r)$ or $M_{do}(r)$ within ~ 7 kpc. To consider the most optimistic case, suppose all the cooled gas at time t_n were distributed uniformly with old stars, $M_{do}(r) \propto M_*(r)$, within 7 kpc, then the central M/L_B would increase from 8.2 to only 8.6. In order to accommodate any increase in M/L_B, it is necessary to assume that the underlying old stars in M87 have M/L_B less than our adopted 8.2 and that the dark dropout has increased it to this value. Finally, mass dropout in the $q = 1$ flow is more spatially diffuse: for optically dark dropout the mass to light ratio within r_b is $M/L_B = 12$ at t_i and $M/L_B = 14$ at $t_n = 13$ Gyrs.

It is well known that thermal conductivity can reduce the cooling rate in the centers of central cD galaxies in galaxy clusters, but the thermal conductivity must be fine-tuned to lower $\dot{M}$ without unrealistically flattening the temperature gradient (Bertschinger & Meiksin 1986; Meiksin 1988; Bregman & David 1988; Rosner & Tucker 1989). We have repeated $q = 1$ and variable $q(r)$ calculations for M87/Virgo, assuming the "alternative" evolution discussed above and including thermal conduction. We assume that the Spitzer or saturated thermal conductivity is reduced uniformly by a factor f to simulate suppression by tangled magnetic fields. In Figure 5 we show that the density and temperature profiles in M87/Virgo can be fit reasonably well with $f = 0.02$ for $q = 1$ flow and $f = 0.08$ for variable q flow. If f is less than these values, the conductivity has little effect and the final flows resemble those described earlier without conduction.

Conductive heating reduces cooling dropout. For the variable q solution with $f = 0.08$ the total mass of cooled gas is 3.1×10^{10} $M_\odot$, about half that without conductivity. Unfortunately, these results are very sensitive to the factor f. The dashed lines in Figure 5 show that if f is changed to 0.05 ($q = 1$) or 0.15 (variable q), the gas temperature is unacceptably high near the center. Since there is no obvious reason why the conductivity should be lower by just the factor f required to reduce $|\dot{M}|$, these models cannot be accepted.

3. NGC 4874 IN COMA

Evidence that the Coma cluster is not in dynamical equilibrium was noticed at *ROSAT* resolution by Briel, Henry & Böhringer (1992) and Briel & Henry (1997) who found significant subclustering and asymmetric temperature variations. Direct *ROSAT* images (Dow & White 1995) and the wavelet analysis of X-ray data by Biviano et al. (1996) clearly show that the center of Coma consists of two subclusters, each centered on the bright cD elliptical galaxies NGC 4489 and NGC 4874, separated in projection by $7.1'$. Recent *XMM* data confirm the existence of enhanced, ~ 100 kpc X-ray emission around these two galaxies (Arnaud et al. 2001; Briel et al. 2001) and so do the *Chandra* images of Vikhlinin et al. (2001). We assume here that the two bright E galaxies are each centers of merging subclusters so the ambient dark matter and gas peaked around each galaxy is locally comoving with the galaxies as they orbit in Coma, i.e. there is no local ram pressure effect near the cD galaxies. The transient, dynamically disturbed nature of Coma is consistent with the observation that Coma is among the minority of clusters that do not have the characteristic centrally peaked X-ray cooling flow structure. In view of the unrelaxed nature of Coma, we begin our gas dynamical calculations at a more recent cosmic time $t_i = 10$ Gyrs, but $t_n - t_i$ is still longer than the relevant sound crossing times.

The gas temperature within a few kpc of NGC 4489 and NGC 4874 decreases dramatically from the virial temperature of the Coma cluster, $T \approx 8 - 9$ keV at $r \gtrsim 7$ kpc to the virial temperature of the embedded galaxy $T \sim 1$ keV at $r \lesssim 4$ kpc. (Arnaud et al. 2001; Vikhlinin et al. 2001). Because of its larger temperature excursion, Coma is a more extreme example of the interaction between cluster and galactic gas than M87/Virgo. Yet, as we show below, the steep temperature gradient observed can also be understood with the classical cooling flow hypothesis. According to the *Chandra* observations of Vikhlinin et al (2001), the emission-weighted temperature near NGC 4874 should increase from

$$\langle T_1 \rangle = 1.0 \pm 0.04 \text{ keV} \quad \text{inside} \quad 7'' \text{ (3.40 kpc)} \qquad (7)$$

to

$$\langle T_2 \rangle = 8.9 \pm 0.4 \text{ keV} \quad \text{in} \quad 10'' - 60'' \text{ (4.86} - \text{29.2 kpc)}. \qquad (8)$$

$\langle T_2 \rangle$ is a line of sight average. In deriving $\langle T_1 \rangle$, Vikhlinin et al. removed background emission from 15 - 30$''$, but not the local background in the 7 - 15$''$region. Nevertheless, $\langle T_1 \rangle$ approximately represents an average temperature over the physical radius interior to $7''$ or 3.4 kpc. We assume a distance to Coma of 106 Mpc based on $H_o = 70$ km s^{-1} per Mpc and v = 7461 km s^{-1} (Faber et al. 1997). At this distance 1″= 0.486 kpc.

3.1. *NGC 4874/Coma Mass Distribution*

The two bright elliptical galaxies in Coma have very similar optical and X-ray properties. However, we concentrate here on NGC 4874 because it is more centrally located (in projection) in the cluster and the surrounding X-ray isophotes are more symmetrical. We assume that the mass distribution is also spherically symmetric about NGC 4874. Since our interest is in the gas flow pattern within ~ 100 kpc from the center of NGC 4874, it is not necessary to approximate the complete mass distribution of Coma with high precision. We adopt a large scale isothermal total mass profile $M_{coma}(r)$ as given in Equation (5) with $M_o = 2.8 \times 10^{14}\ M_\odot$ and core radius $a = 300$ kpc, which is atypically large due to dynamically transient substructure. This mass confines the cluster gas with an X-ray surface brightness distribution similar to that observed by Briel et al. (1992) out to $r \sim 1$ Mpc and beyond. In addition, we adopt an NFW dark matter halo for the galaxy, $M_{4874,nfw} = 1 \times 10^{13}\ M_\odot$, although this mass has almost no effect on our solutions since the galactic virial temperature is so much less than that of the Coma cluster.

The stellar mass distribution is found from the R-band surface brightness measurements of Peletier et al. (1990), which vary linearly with the log of the projected radius R,

$$\mu_R = 17 + 3.125 \log R \qquad \mathrm{mag}/\square''. \tag{9}$$

The corresponding B-band brightness μ_B is found assuming $B - R = 1.67$ typical for E galaxies (Fukugita, Shimasaku & Ichikawa 1995). As before we convert μ_B into physical units and invert with Abel's equation to find the following approximate stellar space density

$$\rho_*(r) = \rho_*(r_b)(r/r_b)^{-0.76} \quad r < r_b \tag{10}$$

$$= \rho_*(r_b)(r/r_b)^{-2.27} \quad r_b < r < r_{max} \tag{11}$$

where $\rho_*(r_b) = 2.137\ M_\odot$ pc^{-3}, $r_b = 2.67''$ (1.30 kpc) is the break radius (Faber et al. 1997) and $r_{max} = 33.71 r_b$. This $\rho_*(r)$ is very close to the stellar mass density shown in Figure 4 of Harris et al (2000) and we have used $M/L_B = 8$ from their paper. The stellar mass distribution of NGC 4874 dominates the gravitational potential in $r \lesssim 12$ kpc.

3.2. *Results*

As before, we begin our NGC4874/Coma calculation by establishing an isothermal gas background in the cluster with temperature $T_{coma} \approx 8 - 9$ keV. Initially the gas is in hydrostatic equilibrium in the approximate dark halo of Coma, $M_{coma}(r)$. At time $t_i = 10$ Gyrs we place NGC 4874 and its dark halo at the center of the cluster, and begin the gas dynamical calculation with the same stellar mass loss and supernova parameters that we used for M87/Virgo. We adopt a more recent starting time $t_i = 10$ Gyrs for NGC4874/Coma because Coma is dynamically unrelaxed compared to M87/Virgo. The temperature T_{coma} and central density $n(0, t_i)$ at time t_i determine the pressure of the cluster gas near NGC 4874 and are adjusted to agree with the large scale gas density distribution in Coma.

For a fully multiphase flow model with $q = 1$, we use $n(0, t_i) = 0.0015$ cm^{-3} and $T_{coma} = 13$ keV (1.5×10^8 K). When $q = 1$, the background cluster temperature must be significantly higher than temperatures observed since the latter also includes cooling gas at every radius. Figure 6 shows the gas electron density and temperature for the $q = 1$ model after it has evolved to time $t_n = 13$ Gyrs. In discussing their *Chandra* observations of NGC 4874, Vikhlinin et al. (2001) show the X-ray surface brightness distribution Σ_x, but not the density profile $n(r)$. Since NGC 4874 was 2.8′ from the center of the *Chandra* field, the spatial resolution is degraded to a half-energy radius of $\sim 0.9''$. Figure 7 shows how the X-ray surface brightness Σ_x (0.2 - 5 keV) of our $q = 1$ solution (solid line) is altered by such a Gaussian point spread function (dashed line) using the integration procedure of Pritchet & Kline (1981). In Figure 7 we plot the (unnormalized) surface brightness observations of Vikhlinin et al. (2001) (circles) and Dow & White (1995) (squares) by adjusting the data vertically for the best fit. The fit is acceptable except perhaps near $R \sim 2 - 3$ kpc where the model emissivity is too high, but this is the region where *Chandra* observations become less accurate in 0.5 - 2 keV.

The physical $T(r)$ and projected $T(R)$ temperature profiles for the $q = 1$ calculation shown in Figure 6 can be used to determine the mean temperatures in the two regions in Equations (7) and (8): $\langle T_1 \rangle = 1.0$ keV and $\langle T_2 \rangle = 7.8$ keV. The latter temperature is less than the value $\langle T_2 \rangle \approx 8.9$ keV observed by Vikhlinin et al. (2001), but is in better agreement with temperatures from Arnaud et al. (2001) in this same region. $\langle T_2 \rangle$ is also much less than the assumed temperature in the background gas, $T_{coma} = 13$ keV. Also shown as filled circles in Figure 6 are local temperatures determined by Vikhlinin et al. which agree rather well with the (unprojected) $T(r)$ in this model.

We also consider an identical flow, but with spatially variable dropout, $q = \exp[-0.05/n(r)]$, and initial density $n(0, t_i) = 0.003$ cm^{-3} and temperature $T_{coma} = 9$ keV. These solutions shown in Figure 8 become essentially single phase ($q \approx 0$) for $r \gtrsim 5$ kpc. Beyond a few kpc the apparent temperature $T(R)$ exceeds the temperature at physical radius $r = R$, $T(r)$, because of line of sight projection. The mean temperature in the two regions as in Equations (7) and (8) are: $\langle T_1 \rangle = 1.0$ keV and $\langle T_2 \rangle = 8.5$ keV. $\langle T_2 \rangle$ is only 0.4 keV less than that observed by Vikhlinin et al., within the margin of observational error. The surface brightness Σ_x (0.2 - 5) keV of this variable q model shown in Figure 7 is also a better fit to the observations at all R.

If the dark and stellar mass of NGC 4874 are ignored as well as stellar mass loss and supernovae, we find that no galactic-scale cooling flow develops in our Coma model even after computing for $t_n - t_i = 13$ Gyrs when the central temperature has dropped by only ~ 0.5 keV below its initial value. Although there is no cluster-scale cooling flow in Coma, more relaxed clusters with $T_{vir} \sim 9$ have higher central densities and can develop cooling flows even without a central cD.

We have also performed NGC 4874/Coma calculations including thermal conductivity as suggested by Vikhlinin et al. (2001). Conduction with unmodified Spitzer and saturated coefficients can definitely be ruled out since the gas temperature remains isothermal at ~ 8 keV throughout NGC 4874 even for large $t_n - t_i$. Our results do not support the suggestion of Vikhlinin et al. that the sharp drop in gas temperature from 8 keV to 1 keV over a few kpc can be understood simply by setting the conductive heat flow (using a conductivity at the classical Spitzer level) at some radius equal to the interior radiative X-ray luminosity near NGC 4874. Instead we find that the coefficients for saturated and unsaturated conduction must be reduced by more than 300 before $\langle T_1 \rangle$ drops below 1.5 keV. As the conductivity is reduced further, our solutions approach the observed $\langle T_1 \rangle = 1$ keV just as the conductivity term in the thermal energy equation becomes too small to influence the temperature profile at all. This result for conduction in NGC 4874/Coma is essentially the same for either constant or variable q flows. We conclude that thermal conduction in NGC 4874/Coma is magnetically suppressed to levels of negligible relevance.

In summary, *Chandra* and *XMM* temperature profiles near NGC 4874 can be fit reasonably well with either constant or variable dropout q, although variable q flows are in better agreement with *Chandra* observations. As with M87/Virgo, the preference between these two models must be based on the evidence in high quality X-ray spectrum for or against multiphase flow.

4. VARIATION OF $\dot{\mathrm{m}}(r)$

As we mentioned in the Introduction, the observed density and temperature profiles can be used to estimate $t_{cool}(r)$ and therefore the integrated mass flow $\dot{M}(r)$ at radius r for steady state cooling flows. Typically, it is found that $\dot{M} \propto r$ for $r < r_b \sim 40 - 120$ kpc (e.g. Allen et al 2001). The decomposition procedure often used by X-ray astronomers to find $\dot{M}(r)$ from the observed $T(r)$ and $n(r)$ is based on dividing the observed cluster into an ensemble of concentric spherical shells and determining the bolometric X-ray emission from each shell, assuming steady state inflow with no stellar mass loss or heating (e.g. Arnaud 1988; Allen et al. 2001). The luminosity of the jth shell is

$$L_j = \Delta \dot{M}_j (H_j + \Delta\Phi_j) + \left[\sum_{i=1}^{j-1} \Delta \dot{M}_i (H_j + \Delta\Phi_j) \right] \quad (12)$$

where $\Delta \dot{M}_j$ is the mass deposited in the jth shell, $H_j = 5kT_j/2\mu m_p$ is the enthalpy of the jth shell and $\Delta\Phi_j$ is the gravitational energy released in crossing the shell. The physical significance of each term is explained in Arnaud (1988). It is interesting to compare the mass flow

$$\dot{M}_{12}(r_j) = \sum_{i=1}^{j-1} \Delta \dot{M}_i$$

found from Equation (12) with $\dot{M}(r)$ from our computed models.

The heavy solid lines in the upper two panels of Figure 9 show $\dot{M}(r) = \rho u 4\pi r^2$ for our $q = 1$ and variable q flows in M87/Virgo at time $t_n = 13$ Gyrs. Also shown are the rates $\dot{M}_{do}(r) = \int_0^r 4\pi r^2 (q\rho/t_{cool}) dr$ that mass is dropping out of the flow (dotted lines); note that this corresponds to the integrated spectroscopic mass deposition rate. If the flow were perfectly steady state $\dot{M}(r)$ and $\dot{M}_{do}(r)$ should be equal as they nearly are for the $q = 1$ solution. For variable q flow, however, $q \approx 0$ beyond $\sim 5 - 10$ kpc, so the integrated dropout mass levels off (dotted line in center panel). For this flow $\dot{M}(r) \approx \dot{M}_{do}(r)$ only holds for $r \lesssim 20$ kpc and beyond this radius they diverge in magnitude and sign because of small deviations from steady flow. The approach to steady flow is accelerated in $q = 1$ flow (upper panel) because mass dropout tends to damp small transient velocities, i.e. dropout makes subsonic flow even more subsonic.

In Figure 9 we also illustrate the mass deposition rate $\dot{M}_{12}(r)$ determined by applying Equation (12) above to our computed flow at time t_n (dashed lines). In solving this equation, we used the same gravitational potential used in our M87 flow calculations and evaluated the enthalpy using the temperature $T_h(r)$ of the background flow at time t_n. For $q = 1$ flow $\dot{M}_{12}(r)$ agrees quite well with both $\dot{M}(r)$ (solid line) and $\dot{M}_{do}(r)$ (dotted line) in spite of the somewhat transient nature of the flow and the presence of stellar mass loss in $r \lesssim 10$ kpc. However, Equation (12) fails to capture either the mass flow or mass deposition profiles in the variable q flow (Fig. 9 center panel). Even when Equation (12) is inaccurate, we seem to find the classic result, $\dot{M}_{12} \propto r$. In the variable q solution beyond about 10 kpc, small undamped radial motions remain at time t_n which have almost no influence on $n(r)$ or $T(r)$, but which radically alter $\dot{M}(r)$. We conclude that Equation (12) is not a reliable means of estimating $\dot{M}(r)$ in clusters that have small deviations from steady flow. Indeed, this may apply to all clusters observed.

For comparison we also plot (lower panel of Figure 9) $\dot{M}(r)$ and $\dot{M}_{do}(r)$ based on a variable q calculation in which the interstellar flow in M87 is computed as an isolated galaxy (as in Brighenti & Mathews 1999), then inserted into Virgo at time $t_i = 6$ Gyrs, i.e. the "alternative" evolutionary model previously discussed. This computational procedure introduces fewer velocity transients. The resulting model generates $n(r)$ and $T(r)$ profiles at time t_n that are virtually identical to those plotted in Figure 2, but the corresponding $\dot{M}(r)$, shown as a solid line in the lower panel of Figure 9, is radically different from $\dot{M}(r)$ in the center panel. $\dot{M}(r)$ in the alternative solution (solid line) lies closer to $\dot{M}_{12}(r)$ (dashed line) but both deviate from the true mass dropout profile $\dot{M}_{do}(r)$ (dotted line). Asymptotically for large $t_n - t_i$, we expect both $\dot{M}(r)$ and $\dot{M}_{12}(r)$ to approach $\dot{M}_{do}(r)$, but this may take longer than a Hubble time. The approximate agreement between $\dot{M}(r)$ and $\dot{M}_{12}(r)$ estimated from Equation (12) in $r \lesssim 50$ may be fortuitous. Equation (12) is nonetheless incapable of accurately detecting the presence of radially dependent $q(r)$ in our models.

Finally, in Figure 10 we show $\dot{M}$, $\dot{M}_{do}$ and $\dot{M}_{12}$ for the two models with thermal conductivity suppression factors f chosen to best fit the $n(r)$ and $T(r)$ data in Figure 5. Both of these are alternative models in which the flow in M87 is computed before inserting into Virgo. When $q = 1$ the conductivity has little effect on the various mass flow rates. But flows with $q = \exp(-0.05/n)$ show that $\dot{M}_{do}$ can be reduced by about 3 from the corresponding calculation without thermal conduction (lower panel in Figure 9). As before, Equation (12) is inaccurate when applied to solutions with variable q and continues to indicate $\dot{M}_{12} \propto r$, predicting mass deposition rates that are much too large.

5. CONCLUSIONS

Recent *Chandra* and *XMM* observations of M87 in the Virgo cluster and NGC 4874 in Coma show that the gas temperature decreases dramatically from the cluster virial temperature (3 or 9 keV respectively) at ~ 50 kpc down to the galactic virial temperature (~ 1 keV) on scales of a few kiloparsecs. We have performed a series of gas dynamical calculations to determine the physical nature of this sharp thermal gradient.

In addition, recent observations have presented somewhat contradictory information about the important question of single phase or multiphase cooling flows. In multiphase flows some of the hot gas cools throughout a large volume to avoid accumulation of large masses of cooled gas right at the center of the flow. Multiphase flow can be identified from spectral observations that show a large range of temperatures at a particular projected radius in the flow, larger than that expected from radial temperature variations projected along the line of sight. As a result of local cooling, gas mass "drops out" from multiphase flows and the gas density in the flow decreases as $(\partial\rho/\partial t)_{do} = -q\rho/t_{cool}$ where t_{cool} is the local radiative cooling time and $0 \leq q(r) \lesssim 1$ is a mass dropout function that is chosen for a best fit to the observations.

Our gas dynamical studies of the interaction of cluster and interstellar gas in cluster-centered cD galaxies are necessarily approximate because of unknown stochastic merging events that may have influenced the cD environment in the past. Nevertheless, it is possible to estimate the flow of cluster gas into central cD galaxies provided the present day properties of the cluster gas have remained approximately constant over times for the flows to become quasi-steady on galactic scales. In most of the gas (cooling) flows calculated here we abruptly place the cD galaxy into the cluster at some time t_i after which there is a transient flow that relaxes to the desired solution after several Gyrs. We have also performed "alternative" evolutionary calculations in which the central cD galaxy evolves by itself from early times, similar to our galaxy group model for NGC 4472 (Brighenti & Mathews 1999), and is placed in the cluster environment at time t_i. The results of these two types of flow calculations are very similar except the total mass of cooled gas is somewhat larger in the alternative flows.

As a result of our calculations for M87/Virgo and NGC4874/Coma, we reach the following conclusions:

(1) The radial variation of gas temperature and density on scales of the cD galaxy can be understood from the usual cooling flow assumptions (e.g. stellar mass loss, spatially distributed mass dropout, etc.) without requiring additional heating sources such as thermal conduction.

(2) If we perform our gas dynamical calculations for the Virgo cluster, assuming isothermal gas at $T \sim 3$ keV with the currently observed large scale density distribution, we find that a fully mature, large scale cooling flow does not develop without the presence of the central cD galaxy. After many Gyrs of calculation, a cD-less single phase flow in the Virgo potential exhibits line of sight averaged gas temperature profiles $T(R)$ with a broad central minimum, but no gas cools. However, a fully complete cosmological calculation of the Virgo cluster is expected to produce a cooling flow with or without a central galaxy (e.g. Suginohara & Ostriker 1998).

(3) In our model for the richer Coma cluster with virial gas temperature ~ 9 keV, we find that the central density is sufficiently low that no cluster scale cooling flow develops in a Hubble time without the central cD. In the presence of the cD galaxy, a cooling flow forms on a galactic scale, just a few kpc in size. This conclusion is probably not general. Since Coma is dynamically disturbed, its current central cluster gas density is atypically low. Relaxed clusters of similar richness have higher central gas densities and may form global cooling flows even without a central cD galaxy.

(4) The radial gas density and temperature profiles in both M87/Virgo or NGC4874/Coma can be understood either in terms of models with large constant mass dropout at every radius ($q = 1$; multiphase flow), or with a variable dropout coefficient $q(r)$ that becomes very small (single phase flow) beyond ~ 10 kpc. High quality X-ray spectra can detect the full range of local temperatures in the flow and thus determine the single or multiphase character of the flow. An observation of the oxygen ratio OVII(0.574 keV)/OVIII(0.652 keV) would be useful to detect gas cooling below 10^6 K. However, currently available *XMM* observations of M87 have been unable to detect unambiguous evidence for multiphase cooling, even in the central regions of M87.

(5) If we insist that the gas must cool somewhere in the flow, we suggest that this occurs within the optical extent of the central cD galaxy where the gas temperature is close to the galactic virial temperature ~ 1 keV. At such low temperatures it is observationally more difficult to detect intrinsic multiphase flow than in hotter gas more distant from the cD. These remarks are specific to NGC4874/Coma and M87/Virgo; in more massive cooling flow clusters, the cooled dropout mass may be distributed over a larger spatial region.

(6) Unfortunately, when most of the radiative cooling is restricted to the central regions of the cD galaxy ($r \lesssim 10$ kpc), the mass of cooled gas there may be inconsistent with mass to light ratios determined from stellar kinematics. At early times when most of the cooling mass dropout occurred, the cooled gas probably formed into luminous stars. Stellar Hβ observations suggest that luminous stars may continue to form from cooling dropout. If the dropout mass is nonluminous, as many authors assume, then it is easy to violate observations of the stellar mass to light ratio unless the nonluminous mass is widely dispersed over the inner ~ 7 kpc in M87.

(7) In this paper we have sought ways to hide the multiphase nature of gas cooling within 10 kpc of the center of M87 and to hide the presence of large masses of optically dark cooled gas there. In spite or our limited success, it is difficult to fully embrace this approach. If M87 were in a much richer cooling flow cluster, it may be impossible to assert that all of the cooled gas accumulates within the central 10 kpc.

(8) We confirm early studies that the coefficient for thermal conductivity must be unrealistically fine-tuned or entirely negligible to lower the mass deposition rate without disagreeing with the observed temperature profiles.

(9) For the cooling flow models considered here we find that the mass flow rate $\dot{M}(r) = \rho u 4\pi r^2$ can be very sensitive to small transient velocities in the flow that have no consequence for $n(r)$ and $T(r)$. Furthermore, the often used Equation (12) is incapable of accurately detecting the presence of radially dependent mass dropout $q(r)$ in flows that are not completely relaxed, which may apply to the majority of cooling flows. In particular, when flows become nearly single phase at large radius, as indicated by recent *XMM* data, our models suggest that $\dot{M}_{12}(r)$ found from Equation (12) predicts a larger mass dropout at the current time than really exists in the flow.

Studies of the evolution of hot gas in elliptical galaxies at UC Santa Cruz are supported by NASA grant NAG 5-3060 and NSF grant AST-9802994 for which we are very grateful. FB is supported in part by grants MURST-Cofin 00 and ASI-ARS99-74.

REFERENCES

Allen, S. W., Fabian, A. C., Johnstone, R. M., Arnaud, K. A., & Nulsen, P. E. J. 2001, MNRAS 322, 589

Arnaud, K. A. 1988, in Cooling Flows in Clusters and Galaxies, ed. A. C. Fabian, Kluwer, Dordrecht, p. 31

Arnaud, M., Aghanim, N., Gastaud, R., Neumann, D. M., Lumb, D., Briel, R., Altieri, B., Ghizzardi, S., Mittaz, J., Sasseen, T. P. & Vestrand, W. T. 2001, A&A 365, L67

Belsole, E., Sauvageot, J. L., Böhringer, H., Worrall, D. M., Matsushita, K., Mushotzky, R. F., Sakelliou, I., Molendi, S., Ehle, M., Kennea, J., Stewart, G., & Vestrand, W. T. 2001 A&A 365 L188

Balbus, S. A. & Soker, N. 1989, ApJ 341, 611

Bertin, G. & Toniazzo, T. 1995, ApJ 451, 111

Bertschinger, E. & Meiksin, A. 1986, ApJ 306, L1

Biviano, A., Durret, F., Gergal, D., Le Fevre, Lobo, C., Mazure, A. & Slezak, E. 1996 A&A 311, 95

Böhringer, H. Belsole, E., Kennea, J., Matsushita, K., Molendi, S., Worrall, D. M., Mushotzky, R. F., Ehle, M., Guainazzi, M., Sakelliou, I., Stewart, G., Vestrand, W. T. & Dos Santos, S. 2001, A&A, 365, L181

Bonamente, M., Lieu, R. & Mittaz, J. P. D. 2001 (astro-ph/0107379)

Bregman, J. N. & David, L. P. 1988, ApJ 326, 639

Bregman, J. N., Miller, E. D. & Irwin, J. A. 2001, ApJ 553, L125

Briel, U. G., Henry, J. P. & Böhringer, H. 1992, A&A 259, L31

Briel, U. G. & Henry, J. P. 1997, in A New Vision of an Old Cluster: Untangling Coma Berenices, eds. F. Durret et al. (astro-ph/9711237)

Briel, U. G., Henry, J. P., Lumb, D. H., Arnaud, M., Neumann, D., Aghanim, N., Gastaud, R., Mittaz, J. P. D., Sasseen, T. P. & Vestrand, W. T. 2001, A&A 365, L60

Brighenti, F. & Mathews, W. G. 1997, ApJ 486, L83

Brighenti, F. & Mathews W. G. 1999, ApJ 512, 65

Brighenti, F. & Mathews, W. G. 2000, ApJ 535, 650

Brighenti, F. & Mathews, W. G. 2002, ApJ (in preparation)

Buote, D. A. 2001, ApJ 548, 652

Buote, D. A. 2000, ApJ 544, 242

Canizares, C. R., Clark, G. W., Jernigan, J. G. & Markert, T. H. 1982, ApJ 262, 33

Ciotti, L.& Ostriker, J. P. 2001, ApJ 551, 131

Dow, K. L. & White, S. D. M. 1995, ApJ 439, 113

Faber, S. M., Tremaine, S., Ajhar, E. A., Byun, Y-I., Dressler, A., Gebhardt, K., Grillmair, C., Kormendy, J., Lauer, T. R. & Richstone, D. 1997, AJ, 114, 1771

Dubinski, J. 1998, ApJ 502, 141

Fabian, A. C., Mushotzky, R. F., Nulsen, P. E. J. & Peterson, J. R. 2001, MNRAS 321, L20

Fabian, A. C. 2001, Oxford Radio Galaxies Conference, Aug. 2000 (astro-ph/0103392)

Fukugita, M., Shimasaku, K. & Ichikawa, T. 1995, PASP 107, 945

Goudfrooij, P., Hansen, L., Jorgensen, H. E., Norgaard-Nielsen, H. U., de Jong, T. & van den Hoek, L. B. 1994, A&AS 104 179

Harris, W. E., Kavelaars, J. J., Hanes, D. A., Hesser, J. E. & Pritchet, C. J. 2000, ApJ 533, 137

Macchetto, F., Marconi, A., Axon, D. J., Capetti, A., Sparks, W. & Crane, P. 1997, ApJ 489, 579

Marconi, A., Axon, D. J., Macchetto, F. D., Capetti, A., Sparks, W. B. & Crane P. 1997, MNRAS 289, L21

Mathews, W. G. & Brighenti, F. 1999, ApJ 527, L31

Mathews, W. G. & Brighenti, F. 2000, ApJ 545, 181

McNamara, B. R., Wise, M. W., David, L. P., Nulsen, P. E. J. & Sarazin C. L. 2000, in "Constructing the Universe with Clusters of Galaxies," IAP, Paris, France July, 2000 (astro-ph/0012331)

Meiksin, A. 1988, in Cooling Flows in Clusters and Galaxies ed. A. C. Fabian, Kluwer:Dordrecht, p. 47

Meiksin, A. 1990, ApJ 352, 466

Merritt, D. & Oh, S. P. 1997, AJ 113, 1279

Molendi, S. & Pizzolato, F. 2001, ApJ (in press) (astro-ph/0106552)

Molendi, S. & Gastaldello, F. 2001, A&A (submitted) (astro-ph/0106553)

Nulsen, P. E. J. 1986, MNRAS 221, 377

Nulsen, P. E. J. & Böhringer, H. 1995, MNRAS 274, 1093

Nulsen, P. E. J. & Fabian, A. C. 1997, MNRAS 291, 425

Oegerle, W. R., Cowie, L., Davidsen, A., Hu, E., Hutchings, J., Murphy, E., Sembach, K. & Woodgate, B. 2001, ApJ (in print) (astro-ph/01206279)

Owen, F. N., Eilek, J. A. & Keel, W. C. 1990, ApJ 362, 449

Owen, F. N., Eilek, J. A. & Kassim, N. E. 2000, ApJ 548, 611

Peletier, R. F., Davies, R. L., Illingworth, G. D., Davis, L. E. & Cawson, M. 1990, AJ 100, 1091

Peterson, J. R., Paerels, F. B. S., Kaastra, J. S., Arnaud, M., Reiprich, T. H., Fabian, A. C., Mushotzky, R. F., Jernigan, J. G. & Sakelliou, I. 2001, A&A 365, L104

Pritchet, C. & Kline, M. I. 1981, AJ 86, 1859

Richstone, D. O. & Tremaine, S. 1986, AJ 92, 72

Rosner, R. & Tucker, W. H. 1989, ApJ 338, 761

Saito, R. & Shigeyama, T. 1999, ApJ 519, 48

Schombert, J. M. 1986, ApJS 60, 603

Soker, N., White, R. E. III, David, L. P. & McNamara, B. R. 2001, ApJ 549, 832

Stone, J. M. & Norman, M. L. 1992, ApJS 80, 753

Suginohara, T. & Ostriker, J. P. 1998, ApJ 507, 16

Thomas, P. A. 1986, MNRAS 220, 949

Thomas, P. A., Fabian, A. C. & Nulsen, P. E. J. 1987, MNRAS 228, 973

Tremaine, S., Richstone, D. O., Byun, Y-I., Dressler, A., Faber, S. M., Grillmair, C., Kormendy, J. & Lauer, T. R. 1994, AJ 107, 634

Tucker, W. H. & Rosner, R. 1983, ApJ 267, 547

Tucker, W. H. & David, L. P. 1997 ApJ 484, 602

van der Marel, R. 1991, MNRAS 253, 710

van der Marel, R. 1994, MNRAS 270, 271

Vikhlinin, A., Markevitch, M., Forman, W. & Jones, C. 2001, ApJ 2001, ApJ 555, L87

White, R. E. III & Sarazin, C. L. 1987, ApJ 318, 629

Xu, H. et al. 2001, (astro-ph/0110013)

Fig. 1.— Gas density and temperature for the $q = 1$ model of M87/Virgo at time t_n. *Upper panel*: Density profiles $n(r)$. *Light solid line*: density of the background hot gas, *heavy solid line*: mean local density including emission from cooling regions. The data are taken from Nulsen & Böhringer (1995). *Lower panel*: Temperature profiles for the $q = 1$ model. *dotted line*: $T_h(r)$, the background, uncooled gas; *light solid line*: $T(r)$, the mean emission-weighted local temperature at physical radius r including cooling regions; *heavy solid line*: $T(R)$ emission-weighted mean of $T(r)$ along the line of sight at projected radius $R = r$. Data are from Molendi & Gastaldello (2001) (*filled circles*) and Böhringer et al. (2001) (*open circles*).

Fig. 2.— Gas density and temperature for the variable q model of M87/Virgo at time t_n. Line types and data are identical to those in Figure 1.

Fig. 3.— Gas density and temperature in M87/Virgo at time t_n for three variants of the variable q model. In the lower panel only the projected mean temperature $T(R)$ is plotted. Data are identical to that in Fig. 1 . *Long dashed lines*: Flow with a more recent initial time $t_i = 10$ Gyrs; *Solid lines*: Flow with stellar M/L_B increased to 16; *Short dashed lines*: Flow with α_* reduced by 2 with $M/L_B = 8$.

Fig. 4.— A comparison of single temperature (1T) spectra (for variable q M87 model) with a composite spectra of a single temperature plus cooling flow (1T + CF) with equal normalizations (for $q = 1$ M87 model). The CF spectrum extends from T_h down to 0.1 keV. *Upper panel*: Spectra at $R \approx 30$ kpc: (1T + CF) composite spectrum for gas at $T_h = 3$ keV (solid line); 1T spectrum for gas at average temperature $T = 2.5$ keV (dotted line). *Lower panel*: $R \approx 1$ kpc: (1T + CF) composite spectrum for gas at $T_h = 0.95$ keV (solid line); 1T spectrum for gas at $T = 0.8$ keV (dotted line).

Fig. 5.— Gas density and temperature profiles for M87/Virgo at time t_n including thermal conductivity reduced at all radii from the Spitzer or saturated value by a factor f. *Upper panel*: The effective density profile $n(r)$ corresponding to emission from background and cooling gas. Variable q flow for $f = 0.02$: (*heavy solid line*) and $f = 0.05$ (*heavy dashed line*); Flow with $q = 1$ for $f = 0.08$: (*light solid line*) and $f = 0.15$ (*light dashed line*); *Lower panel*: Projected temperature $T(R)$ profiles; line types are identical to those in the upper panel.

Fig. 6.— Gas density and temperature in the $q = 1$ model for NGC4874/Coma at time t_n. *Upper panel*: Density profiles $n(r)$ with solid curves labeled as in Fig. 1. *Long dashed line*: β-model gas profile from Briel et al. (1992) appropriate for large r. *Lower panel*: Temperature profiles for $T_h(r)$, $T(r)$ and $T(R)$ labeled as in Fig. 1. Data are from Arnaud et al. (2001) (*open circles*) and Vikhlinin et al. (2001) (*filled circles*).

Fig. 7.— X-ray surface brightness distribution $\Sigma_x(R)$ (0.5 - 2 keV) at t_n in NGC4784/Coma before (*solid lines*) and after convolution with *Chandra* PSF (*dashed lines*). *Upper panel*: For $q = 1$ flow; *Lower panel*: For variable q flow. Circles are *Chandra* data from Vikhlinin et al. (2001) and squares are *ROSAT* data from Dow & White (1995).

Fig. 8.— Gas density and temperature in the variable q model for NGC4874/Coma at time t_n. Line types and data are identical to those in Figure 6.

Fig. 9.— Mass flows in M87. Variation of $\dot{M}(r) = \rho u 4\pi r^2$ in computed models (*solid lines*), $\dot{M}_{12}(r)$ from Equation (12) (*dashed lines*) and integrated rate of cooling dropout $\dot{M}_{do}(r)$ (*dotted lines*), all evaluated at time $t_n = 13$ Gyrs. *Upper panel*: For the $q = 1$ solution. *Center panel*: For the variable q solution. $\dot{M}(r)$ computed from the model (solid line) changes sign and becomes positive (outflow) for $r > 53$ kpc. *Lower panel*: An alternative variable q solution at t_n in which M87 is evolved separately, then inserted into Virgo at $t_i = 6$ Gyrs.

Fig. 10.— Radial variation of $\dot{M}(r)$ (*solid lines*), $\dot{M}_{do}(r)$ (*dotted lines*) and $\dot{M}_{12}(r)$ (*dashed lines*) for flows with thermal conductivity reduced by a factor f. *Upper panel*: $q = 1$ flow with $f = 0.02$; *Lower panel*: variable q flow with $f = 0.08$.

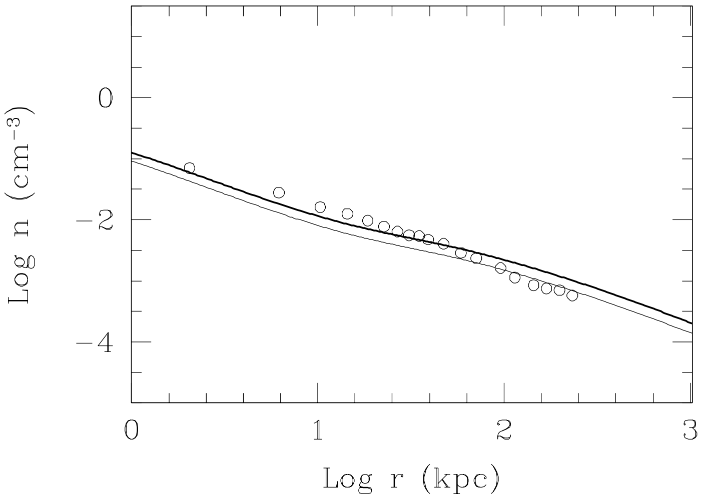
Log n (cm^{-3})
0
−2
−4
0
1
2
3
Log r (kpc)

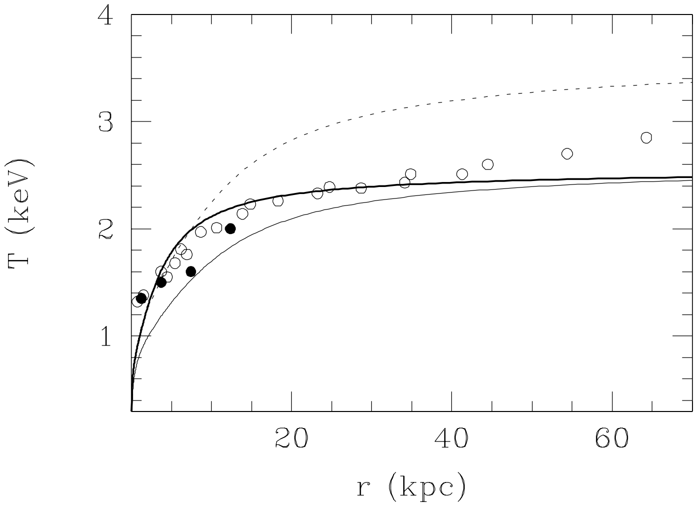
T (keV)
4
3
2
1
20
40
60
r (kpc)

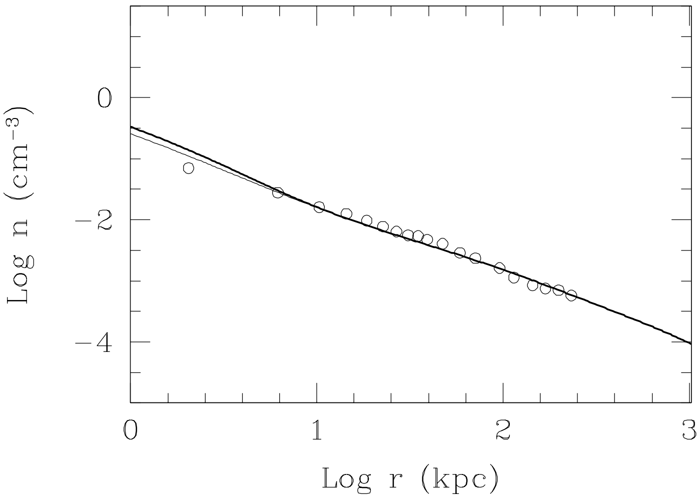

Log n (cm^{-3})
0
−2
−4
0
1
2
3
Log r (kpc)

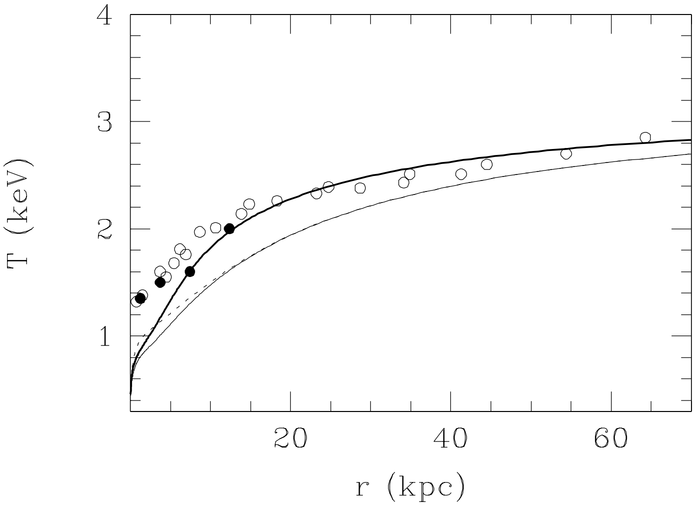

T (keV)
4
3
2
1
20
40
60
r (kpc)

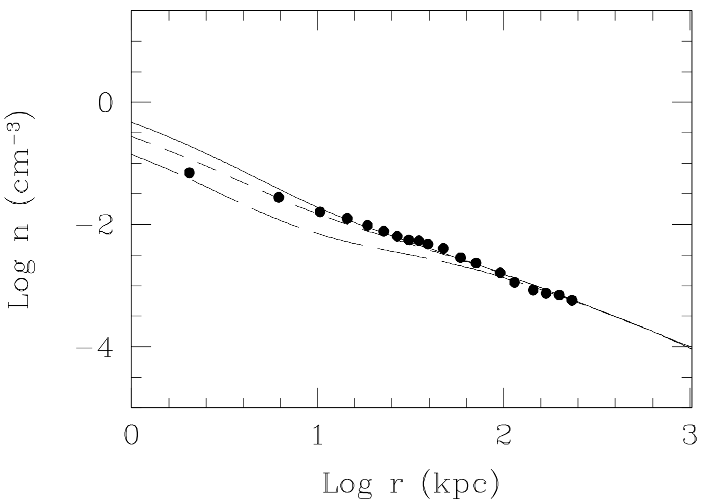
0
−2
−4
0
1
2
3
Log n (cm⁻³)
Log r (kpc)

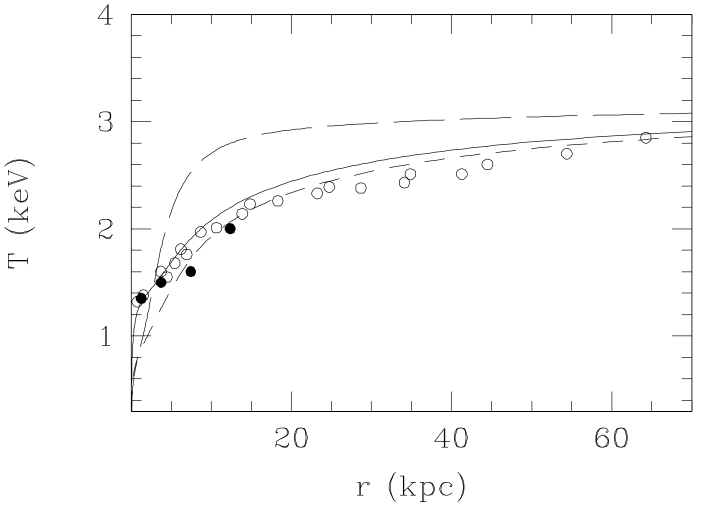
4
3
2
1
20
40
60
T (keV)
r (kpc)

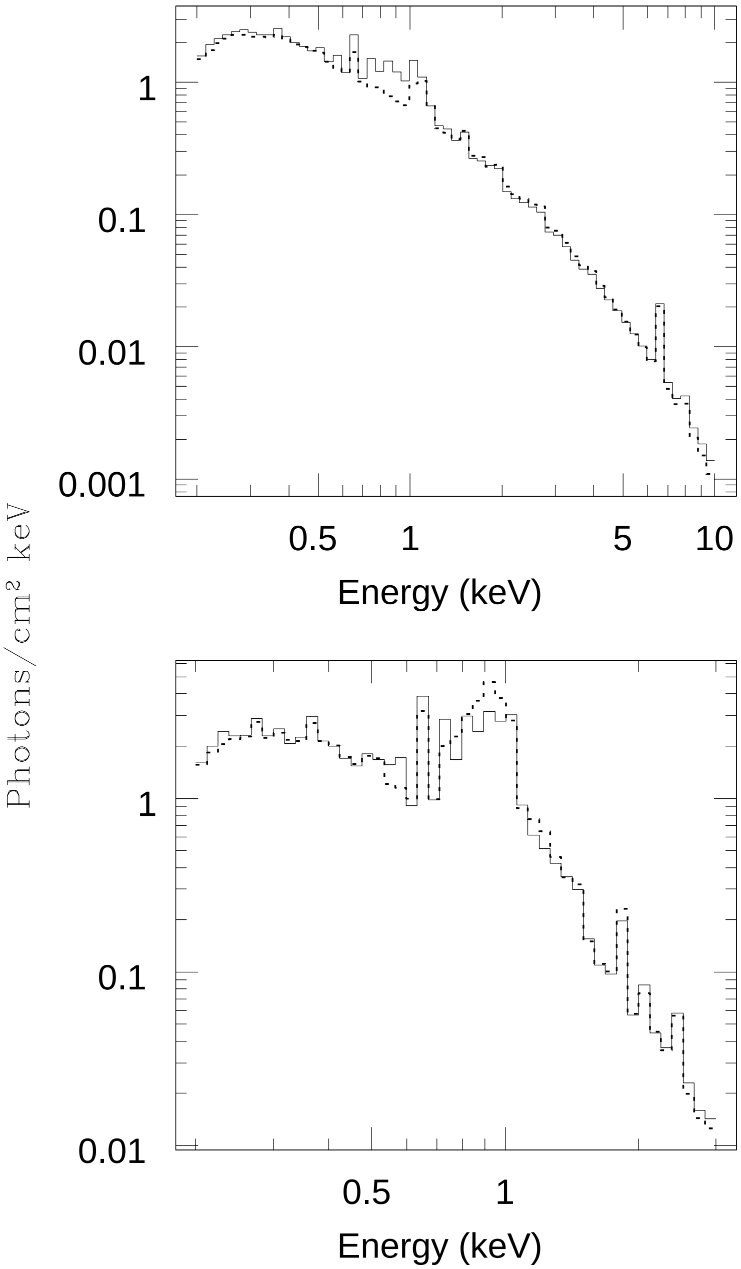
Photons/cm² keV
1
0.1
0.01
0.001
0.5
1
5
10
Energy (keV)
1
0.1
0.01
0.5
1
Energy (keV)

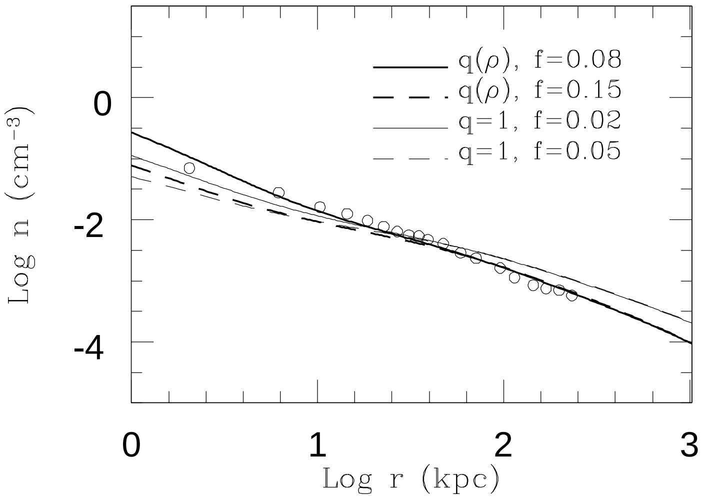
q(ρ), f=0.08
q(ρ), f=0.15
q=1, f=0.02
q=1, f=0.05
Log n (cm⁻³)
0
-2
-4
0
1
2
3
Log r (kpc)

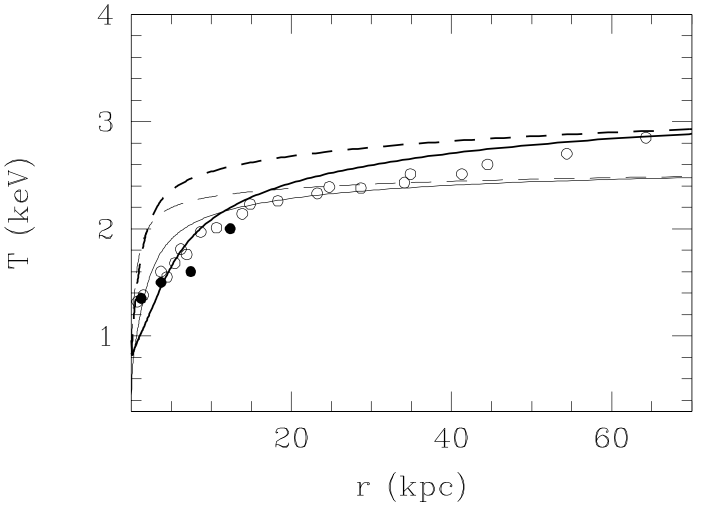
T (keV)
4
3
2
1
20
40
60
r (kpc)

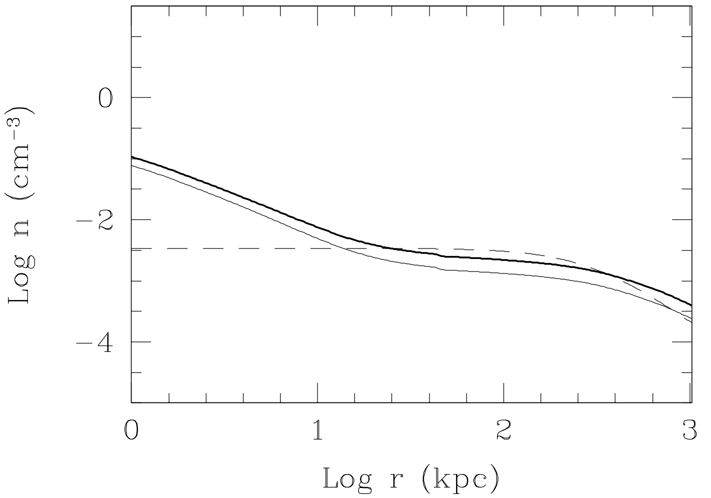

Log n (cm^{-3})
0
−2
−4
0
1
2
3
Log r (kpc)

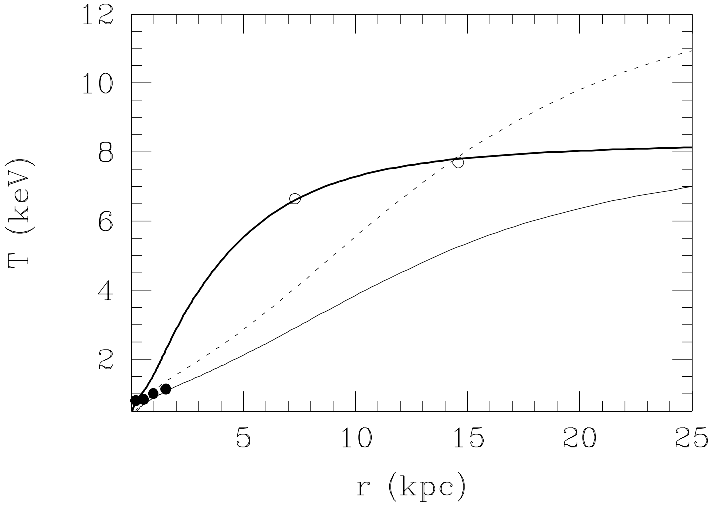

T (keV)
12
10
8
6
4
2
5
10
15
20
25
r (kpc)

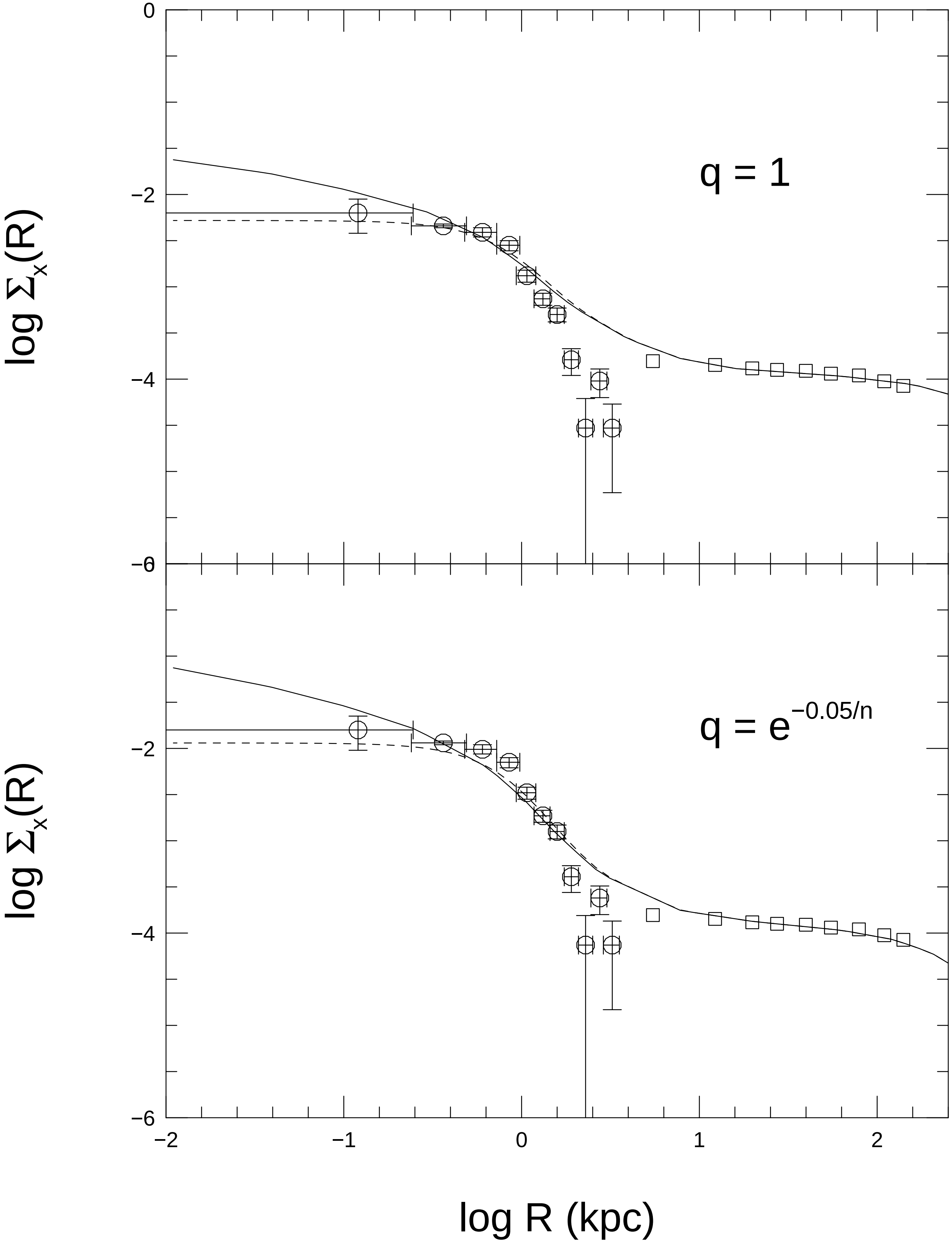
q = 1
$q = e^{-0.05/n}$
log Σx(R)
log Σx(R)
log R (kpc)
0
−2
−4
−6
−2
−4
−6
−2
−1
0
1
2

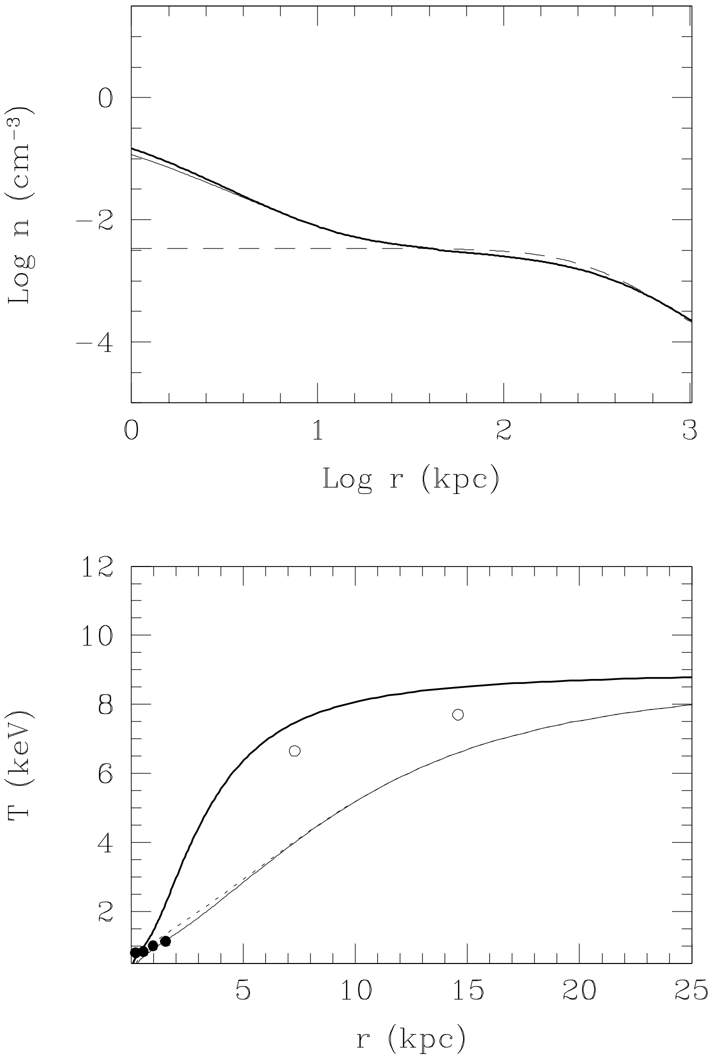
Log n (cm^{-3})
0
−2
−4
0
1
2
3
Log r (kpc)
T (keV)
12
10
8
6
4
2
5
10
15
20
25
r (kpc)

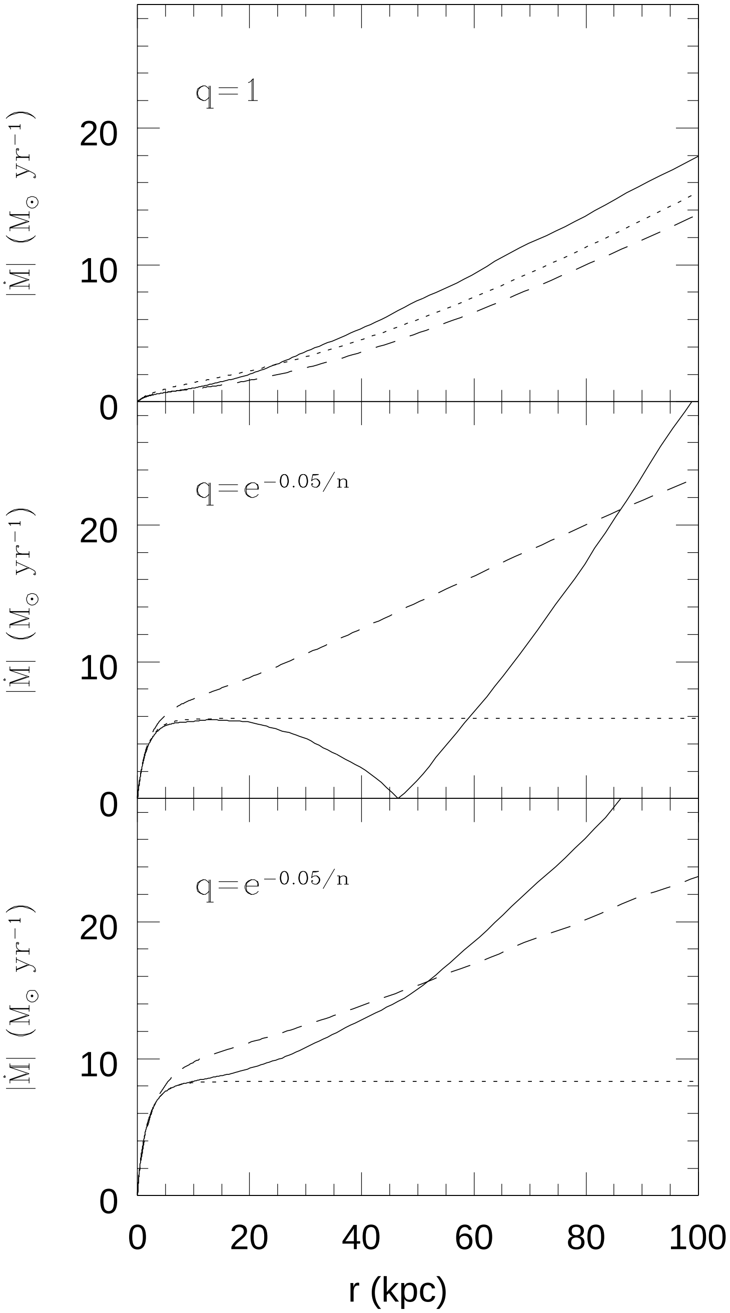
q=1
$q=e^{-0.05/n}$
$q=e^{-0.05/n}$
$|\dot{M}|\ (M_\odot\ yr^{-1})$
$|\dot{M}|\ (M_\odot\ yr^{-1})$
$|\dot{M}|\ (M_\odot\ yr^{-1})$
0
10
20
0
10
20
0
10
20
0
20
40
60
80
100
r (kpc)

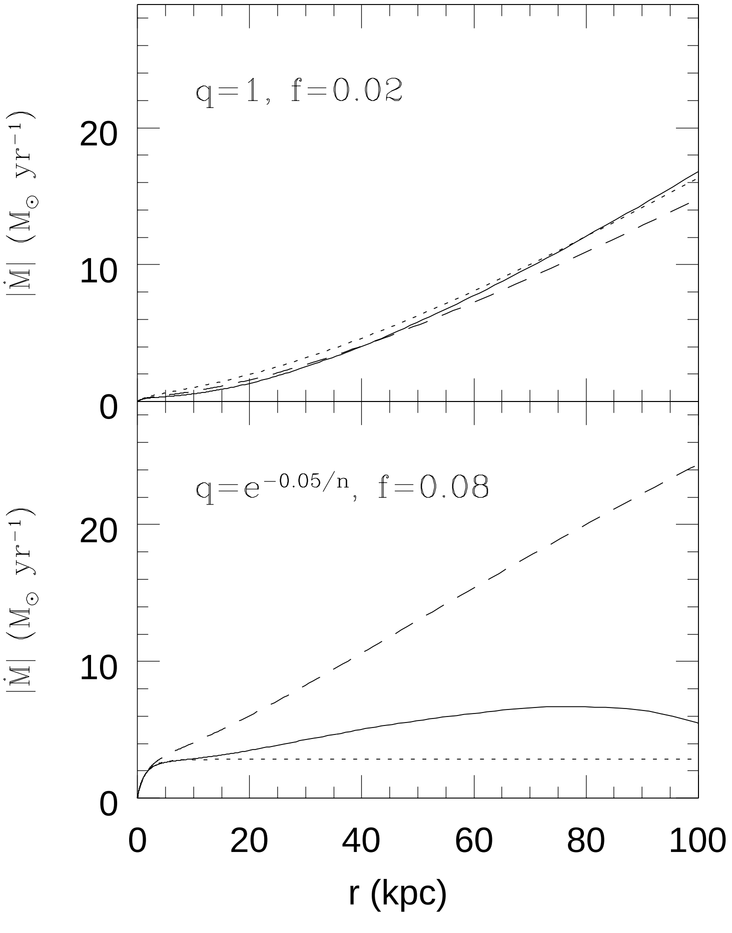
q=1, f=0.02
$q=e^{-0.05/n}$, f=0.08
$|\dot{M}|$ ($M_\odot$ yr^{-1})
$|\dot{M}|$ ($M_\odot$ yr^{-1})
0
10
20
0
10
20
0
20
40
60
80
100
r (kpc)